ARTICLE

Using Ion-velocity Map Imaging Technique to Study Photodissociation of 2-Bromopentane

Zhong Gu, Min Chen, Chao He, Xi-lin Bai, Rui Mao*, Qun Zhang*, Yang Chen*

Hefei National Laboratory for Physical Sciences at the Microscale and Department of Chemical Physics, University of Science and Technology of China, Hefei 230026, China

(Dated: Received on May 9, 2013; Accepted on May 21, 2013)

The photodissociation dynamics of 2-bromopentane at ∼234 nm has been investigated by utilizing ion-velocity map imaging technique. The mapped images of $Br(^2P_{3/2})$ (denoted as Br) and $Br(^2P_{1/2})$ (denoted as Br*) fragments were analyzed by means of the speed and angular distributions, respectively. The speed distributions can be fitted with two Gaussian components which are correlated to the two independent reaction paths on the excited potential energy surfaces (PES). The high-energy component is from the prompt dissociation along the C−Br stretching mode, while the low-energy one is related to the dissociation from the coupling of the C−Br stretching and bending modes. Relative quantum yield is measured to be 0.892 for Br in the photodissociation of 2-bromopentane at 234 nm. Combining the anisotropy parameter with the relative quantum yield of Br and Br* fragments, the contributions of the excited $^3Q_0$, $^3Q_1$, and $^1Q_1$ states to the products Br and Br* were derived. The effect of alkyl branching on the mechanism of photodissociation was discussed by comparing the photodissociation processes of four isomers of bromopentane.

Key words: Ion-velocity imaging, Photodissociation, 2-Bromopentane

I. INTRODUCTION

Chemists pay substantial attention to the photolysis mechanism of alkyl bromides because of their importance in stratospheric ozone depletion [1, 2]. The first ultraviolet absorption band (the A band) of alkyl bromides consists of three overlapping excited states, $^3Q_1$, $^3Q_0$, and $^1Q_1$ in Mulliken's notation [3]. The A band is formed via an $\sigma^*\leftarrow$n transition localized on the C−Br bond, so photodissociation via excitation to the A band of alkyl bromides produces bromine atoms in the ground state $Br(^2P_{3/2})$ (denoted as Br) and bromine atoms in the excited state $Br(^2P_{1/2})$ (denoted as Br*) [3]. The $^3Q_0$ state correlates to the Br* product and the corresponding transition is aligned parallel to the C−Br bond axis, while the $^3Q_1$ and $^1Q_1$ states produce Br through perpendicular transition [3].

In recent years, plenty of research has been completed on the photodissociation dynamics of a range of alkyl bromides [4−14] by the time-sliced ion velocity imaging technique [15−17]. From the analyses of the photodissociation processes of the alkyl bromides, different mechanisms have been concluded. For CH_3Br [4], C_2H_5Br [5], *n*-C_3H_7Br [6], *iso*-C_3H_7Br [7], *n*-C_4H_9Br [8, 9], *iso*-C_4H_9Br [10], *n*-$C_5H_{11}Br$ [12], the images of the Br and Br* fragments show the characteristics of a prompt dissociation along the C−Br stretching mode. While other molecules, such as *tert*-C_4H_9Br [10], 2-C_4H_9Br [11], *tert*-$C_5H_{11}Br$ [13, 14], *neo*-$C_5H_{11}Br$ [14], exhibit one or two more independent dissociation pathways besides the direct one, which are related to the coupling of bending modes and C−Br stretching mode. The carbon-chain branching can make sense in the dissociation process to produce Br and Br* fragments for alkyl bromides. Now, the question is how the alkyl branching affects the mechanism of photodissociation. To solve the problem, more research and analyses are needed. Therefore, we focus our attention on 2-bromopentane which has two branches on the α carbon atom. In this work, we present the photodissociation dynamics of 2-bromopentane at ∼234 nm.

II. EXPERIMENTS

The experiments were carried out using a home-built time-sliced ion velocity imaging apparatus [18]. Briefly, 2-bromopentane which was seeded in He (∼2%) at a stagnation pressure of ∼3 atm was expanded through a pulsed nozzle (Series 9, General Valve) with an orifice diameter of 0.5 mm in a source chamber and skimmed to form a supersonically molecular beam into a differentially pumped detection chamber. The operating pressures in the source and detection chambers were maintained at $\sim10^{-6}$ and $\sim2\times10^{-7}$ Torr, respectively. After passing through a 1.5 mm hole in the repeller plate, the molecular beam directed along the time-of-

*Authors to whom correspondence should be addressed. E-mail: maorui@ustc.edu.cn, qunzh@ustc.edu.cn, yangchen@ustc.edu.cn

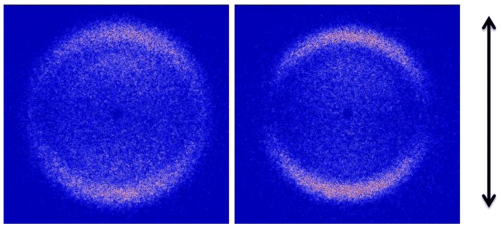

FIG. 1 The raw images of Br and Br* fragments following the photodissociation of 2-$C_5H_{11}Br$. (a) Br at 233.62 nm, (b) Br* at 233.95 nm. The arrow shows the linear polarization direction of the dissociation laser which is parallel to the vertical direction of the image plane.

flight (TOF) axis was intersected at right angles by the laser beam in the detection zone. The ∼234 nm laser is the output of a neodymium-doped yttrium aluminum garnet (Nd:YAG) (GCR-170, Spectra Physics) pumped dye laser (Precision Scan, Sirah) and focused by a f=210 mm lens. The electric vector of the linearly polarized laser was set perpendicularly to the TOF axis and thus parallel to the front face of the micro channel plates (MCP's).

Br and Br* were probed at 233.62 and 233.95 nm (usually denoted as 234 nm) via the $6p(^4P_{1/2})\leftarrow 4p^5(^2P_{3/2})$ and $6p(^2S_{3/2})\leftarrow 4p^5(^2P_{1/2})$ transitions, respectively, using a (2+1) REMPI method. Within a set of ion optics designed for the ion velocity imaging measurements, the Br^+ ions were accelerated by the focusing electric fields and projected onto a 40 mm-diameter Chevron-type dual MCP's coupled to a P-47 phosphor screen (APD 3040FM, Burle Electro-Optics). A fast high-voltage switch (PVM-4210, DEI; typical duration ∼80 ns) was pulsed to gate the gain of the MCP's for mass selection as well as the time slicing of the ion packet. The transient images from the phosphor screen were captured by a charge-coupled device (CCD) camera (Imager Compact QE 1376×1024 pixels, LaVision) and transferred to a computer on an every shot basis for event counting [19] and data analysis. Timing of the pulsed nozzle, laser, and gate pulse applied on the MCP's was controlled by two multichannel digital delay pulse generators (SRS, DG 535).

III. RESULTS

Figure 1 shows the images of Br and Br* obtained from the photodissociation of 2-bromopentane at 233.62 and 233.95 nm. The polarization vector of the photolysis laser is parallel to the vertical direction of the image plane.

The velocity distribution of bromine fragments, $P(v)$, was extracted by integrating the reconstructed three-dimensional distribution over all angles at each speed, as shown in Fig.2. Fitting with a Gaussian function,

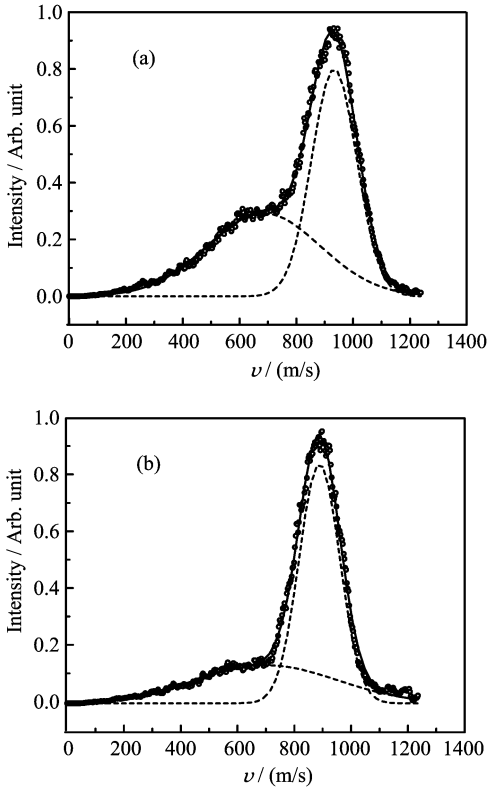

FIG. 2 The velocity distributions of (a) Br at 233.62 nm and (b) Br* at 233.95 nm following the photodissociation of 2-$C_5H_{11}Br$. The circle symbols represent the experimental results, the solid lines are the sum of the simulated distributions, and the broken lines show the Gaussian-fitting lines.

the speed distributions of Br and Br* were separated into two components. The center-of-mass translational energy distribution $P(E)$, was obtained by converting the speed distribution using the following equations

$$P(E) = P(v)\frac{\mathrm{d}v}{\mathrm{d}E} \tag{1}$$

$$E_\mathrm{t} = \frac{1}{2}(m_\mathrm{Br} + m_{\mathrm{C_5H_{11}}}) \times \frac{m_\mathrm{Br}}{m_{\mathrm{C_5H_{11}}}} \times v_\mathrm{Br}^2 \tag{2}$$

where $P(E)$, $P(v)$, E_t, m_Br, $m_{\mathrm{C_5H_{11}}}$, and v_Br denote the energy distribution, the speed distribution, the total translational energy, the mass of Br, the mass of C_5H_{11}, and the velocity of the bromine fragments, respectively.

The value of f_T, which denotes the fraction of E_t to the available energy E_avail, can be obtained with the following equations

$$f_\mathrm{T} = \frac{E_\mathrm{t}}{E_\mathrm{avail}} \tag{3}$$

$$\begin{aligned} E_\mathrm{avail} &= h\nu - D_0 - E_\mathrm{el} + E_\mathrm{int}^\mathrm{P} \\ &= E_\mathrm{t} + E_\mathrm{int} \end{aligned} \tag{4}$$

where $h\nu$, D_0, E_el, $E_\mathrm{int}^\mathrm{P}$, and E_int denote the photon energy, the C−Br bond dissociation energy (296.6 kJ/mol

DOI:10.1063/1674-0068/26/05/493-497

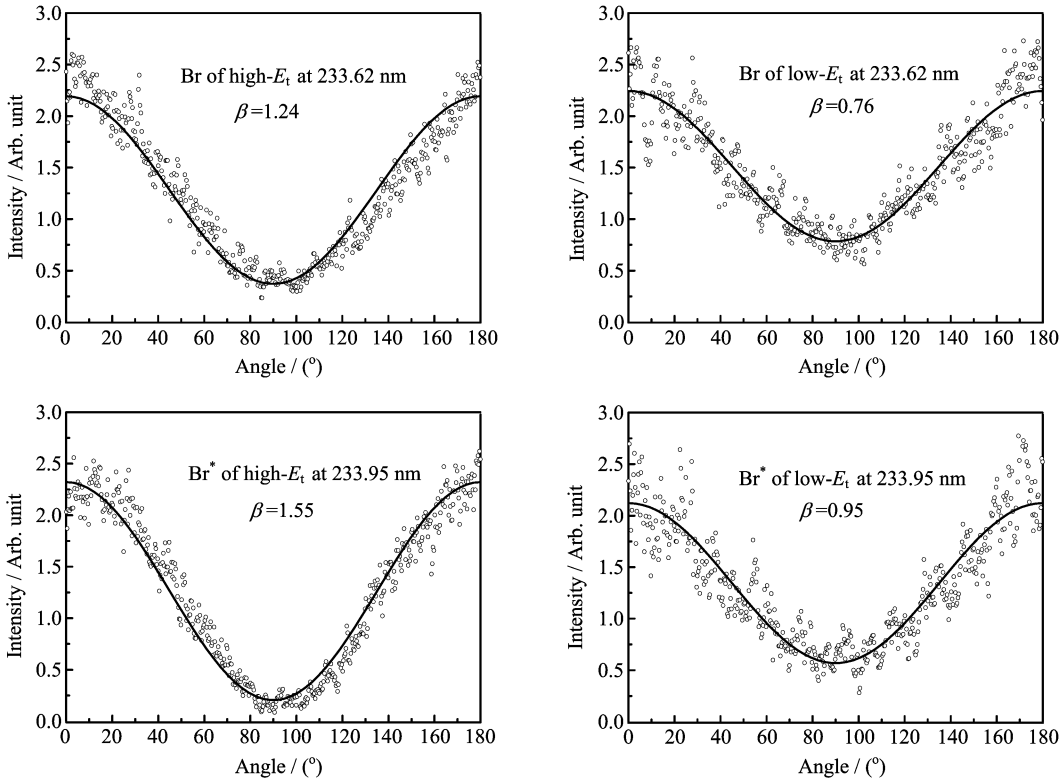

FIG. 3 The angular distributions of Br and Br* following the photodissociation of 2-$C_5H_{11}Br$. The circle symbols represent the experimental data, and the solid lines show the best-fitting profiles.

TABLE I Energy partitioning, anisotropy parameters, and relative contribution of each component in 2-C_5H_{11}+Br (Br*) channel.

Wavelength/nm	Product	$h\nu$	E_{avail}/(kJ/mol)	E_t/(kJ/mol)	f_T	β	Relative contribution
233.62	Br	512.1	215.5	72.2	0.34	1.24	0.53
				38.6	0.18	0.76	0.47
233.95	Br*	511.3	170.7	66.1	0.39	1.55	0.65
				36.4	0.21	0.95	0.35

[20]), the electronic energy level of the bromine atom (0 kJ/mol for Br and 44 kJ/mol for Br*), the internal energy of parent molecules, and the internal energy of 2-C_5H_{11} radical, respectively. The values of E_t and f_T together with the relative contribution of each gaussian component are listed in Table I.

The angular distribution $P(\theta)$ of the bromine fragments in Fig.3 was extracted by integrating a three-dimensional distribution within a certain range of speed at each angle. The anisotropy parameter β was fitted using the standard formula [21],

$$P(\theta) \propto 1 + \beta P_2(\cos\theta) \tag{5}$$

where $P_2(\cos\theta)$ is the second-order Legendre polynomial and the parameter θ is the angle between the laser polarization and the recoil axis of the bromine fragments (C−Br). The β values for Br and Br* are listed in Table I.

The branching ratio $N(Br^*)/N(Br)$ can be expressed by the equation

$$\frac{N(Br^*)}{N(Br)} = k\frac{S(Br^*)}{S(Br)} \tag{6}$$

where $N(X)$ is number of species X, $S(X)$ is the measured mass spectrum signal intensity of species X, and k is the proportional constant. The k value is determined by the probability ratio of resonance-enhanced multiphoton ionization, relative detection efficiencies, and other instrument factors. By performing a calibration experiment of Br_2 photolysis under the same condition [22], the value of k at 234 nm is found to be 0.37. The ratio of $N(Br^*)/N(Br)$ is obtained to be 0.121 at 234 nm for 2-bromopentane.

The relative quantum yields of $\Phi(Br)$ and $\Phi(Br^*)$ can be obtained from the product ratio according to the

DOI:10.1063/1674-0068/26/05/493-497

TABLE II The parallel and perpendicular weighting factors of the high-E_t components for the photodissociation of 2-$C_5H_{11}Br$ at 234 nm and the contribution of each excited state to the Br and Br* formation at 234 nm.

Wavelength/nm	Product	Φ	β	$\chi_{//}$	$\chi_\perp$	Initial excitation	Curve crossing
233.62	Br	0.892	1.24	0.75	0.25	$f(^1Q_1)+f(^3Q_1)=0.223$	$f(^1Q_1\leftarrow{}^3Q_0)=0.669$
233.95	Br*	0.108	1.55	0.85	0.15	$f(^3Q_0)=0.092$	$f(^3Q_0\leftarrow{}^1Q_1)=0.016$

following relations

$$\Phi(\mathrm{Br}^*) = \frac{N(\mathrm{Br}^*)}{N(\mathrm{Br}) + N(\mathrm{Br}^*)} \tag{7}$$

$$\Phi(\mathrm{Br}) = 1 - \Phi(\mathrm{Br}^*) \tag{8}$$

The resultant relative quantum yield of Φ(Br) is 0.892 at 234 nm, shown in Table II.

IV. DISCUSSION

The two Gaussian components, shown in the speed distributions of Br and Br* atoms, indicate that there are two independent reaction paths on the photodissociation dynamics of 2-bromopentane at 234 nm. The fractions of the high-E_t components are 53% and 65% for Br and Br*, respectively. It can be explained reasonably by the classic impulsive model, related to the prompt dissociation along the C−Br stretching mode [23]. The radical limits of the prompt dissociation can be described in two cases, the soft radical limit and the rigid model. The soft radical limit accounts for vibrational excitation while the rigid model ignores it. The values of E_t/E_{avail} corresponding to the soft and rigid radical limit are 0.28 and 1, respectively [12]. In this work, the values of E_t/E_{avail} for the high-E_t channels of Br and Br* are 0.34 and 0.39 (shown in Table I), respectively, close to the soft radical limit. Therefore, it is reasonable that the high-E_t channels of Br and Br* come from the direct dissociation along the C−Br bond. However, the low-E_t components of Br and Br* cannot be accommodated by the prompt impulsive dissociation, as the values of E_t/E_{avail} are 0.18 and 0.21 (shown in Table I), respectively, lower than that of the soft radical limit (0.28). The dissociation is no longer solely ascribed to the C−Br stretching mode but also ascribed to the coupling of bending mode and C−Br stretching mode. We attributed the low-E_t components to the dissociation from the coupling of the C−Br stretching and bending modes. The bending-stretching motions have been observed widely in recent reports of photodissociation experiments, such as *tert*-C_4H_9Br [10], 2-C_4H_9Br [11], *tert*-$C_5H_{11}Br$ [13, 14], *neo*-$C_5H_{11}Br$ [14]. Our results for the low-E_t components are very close to that observed in the experiments of *tert*-$C_5H_{11}Br$ and *neo*-$C_5H_{11}Br$. Hence, the explanation of the low-E_t dissociation channel is reasonable.

To investigate the photodissociation mechanism of 2-bromopentane at 234 nm, we need to analyze the anisotropy parameter as well. The relative contributions of the parallel and perpendicular transitions to the anisotropy parameters β can be analyzed using the following classical relationship,

$$\beta = \chi_{//}\beta_{//} + \chi_\perp\beta_\perp \tag{9}$$

$$\chi_{//} + \chi_\perp = 1 \tag{10}$$

where $\beta_{//}$=2 and $\beta_\perp$=−1 are the limit values for the pure parallel transition and the pure perpendicular transition, respectively. $\chi_{//}$ and $\chi_\perp$ are the parallel and perpendicular weighting factors.

For the high-E_t channel of Br and Br*, β are 1.24 and 1.55, respectively (in Table I). As listed in Table II, the $\chi_{//}$ values for Br and Br* fragments are 0.75 and 0.85. This indicates that the parent molecule is mainly excited to the $^3Q_0$ state by parallel transition leading to the Br* product. However, the Br fragment is the main product actually, which is supposed to come from the $^3Q_1$ and $^1Q_1$ states through perpendicular transition. Considering the crossing among the excited states, we expect that the nonadiabatic $^1Q_1\leftarrow{}^3Q_0$ transition plays an important role for Br* and Br fragments in the dissociation process of 2-$C_5H_{11}Br$. The relative fractions of individual pathways to produce Br and Br* can be obtained using the following relation [12, 20],

$$\begin{pmatrix} \Phi_{\mathrm{Br}}\chi_{\mathrm{Br}//} & \Phi_{\mathrm{Br}}\chi_{\mathrm{Br}\perp} \\ \Phi_{\mathrm{Br}^*}\chi_{\mathrm{Br}^*//} & \Phi_{\mathrm{Br}^*}\chi_{\mathrm{Br}^*\perp} \end{pmatrix} = \\ = \begin{pmatrix} f\left(^3Q_0 \leftarrow{}^1 Q_1\right) & f(^1Q_1) + f(^3Q_1) \\ f\left(^3Q_0\right) & f\left(^1Q_1 \leftarrow {}^3Q_0\right) \end{pmatrix} \tag{11}$$

where $\chi_{\mathrm{Br}//}$, $\chi_{\mathrm{Br}\perp}$, $\chi_{\mathrm{Br}^*//}$, $\chi_{\mathrm{Br}^*\perp}$ represent the portion of Br and Br* which come from a parallel or perpendicular transition, Φ_{Br} and Φ_{Br^*} are relative quantum yields listed in Table II, and $f\left(^3Q_0\leftarrow{}^1Q_1\right)$, $f(^1Q_1)$, $f(^3Q_1)$, $f(^3Q_0)$, and $f(^1Q_1\leftarrow{}^3Q_0)$ are contributions of the individual pathway. The probability of the nonadiabatic $^1Q_1\leftarrow{}^3Q_0$ curve crossing, $f(^1Q_1\leftarrow{}^3Q_0)$ was determined to be 0.669.

In our experiment, the images of Br and Br* of 2-$C_5H_{11}Br$ show two rings which are related to two independent dissociation channels. We compared our results with that of three other isomers of bromopentane [12, 14] to confirm the effect of alkyl branching on the mechanism. Unlike the unbranched *n*-$C_5H_{11}Br$ molecule where only a direct fission of the C−Br bond is involved, the branched *neo*-$C_5H_{11}Br$, *tert*-$C_5H_{11}Br$ and 2-$C_5H_{11}Br$ molecules exhibit one or two more in-

DOI:10.1063/1674-0068/26/05/493-497

dependent dissociation pathways with much energy being decayed via an extensive excitation of the bending modes of the parent molecules prior to the C−Br bond fission. This observation strongly suggests that the dissociation coordinate for the two carbon-chain branched molecules is no longer solely ascribed to the C−Br stretching mode but rather a combination of the bending-stretching modes. Moreover, the relative quantum yield is also affected by the alkyl branching, as the relative quantum yield of $Br(^2P_{3/2})$ of n-$C_5H_{11}Br$ is far smaller than the other three isomers. The more branched carbon chain leads to more vibrational excitation in the photodissociation process, and the characteristic of multi-dimensional dissociation becomes apparent.

V. CONCLUSION

The Br atom formation dynamics of 2-bromopentane at 233.62 and 233.95 nm has been studied by means of ion-velocity map imaging technique. Two dissociation channels in the photodissociation process of 2-bromopentane are suggested. The channel of high-E_t component is related to the prompt dissociation along the C−Br stretching mode, and the channel of low-E_t component is related to the dissociation along the C−Br stretching mode, coupling with bending modes. Relative quantum yield is derived to be 0.892 for Br at 234 nm. The contributions of the excited $^3Q_0$, $^3Q_1$, and $^1Q_1$ states to the products (Br and Br*) were extracted using the anisotropy parameter β and relative quantum yield Φ of Br and Br* fragments. The effect of alkyl branching on the mechanism of photodissociation was discussed by comparing the photodissociation processes of four isomers of bromopentane.

VI. ACKNOWLEDGMENTS

This work was supported by the National Natural Science Foundation of China (No.21273212), the China Postdoctoral Science Foundation (No.2013M531506), the Ministry of Science and Technology of China (No.2007CB815203 and No.2010CB923302), the Chinese Academy of Sciences (No.KJCX2-YW-N24 and No.KJCX2-EW-W09), the Fundamental Research Funds for the Central Universities of China (No.WK2340000012), and the USTC-NSRL Joint Funds (No.KY2340000021).

[1] Y. L. Yung, J. P. Pinto, R. J. Watson, and S. P. Sander, J. Atmos. Sci. **37**, 339 (1980).
[2] R. P. Wayne, *The Chemistry of Atmospheres*, 2nd Edn., New York: Oxford University Press, (1991).
[3] R. S. Mulliken, J. Chem. Phys. **8**, 382 (1940).
[4] T. Gougousi, P. C. Samartzis, and T. N. Kitsopoulos, J. Chem. Phys. **108**, 5742 (1998).
[5] Y. Tang, L. Ji, and B. Zhang, Chem. Phys. Chem. **6**, 2137 (2005).
[6] S. Zhang, Y. M. Wang, B. F. Tang, Q. S. Zheng, and B. Zhang, Chem. Phys. Lett. **413**, 129 (2005).
[7] R. Zhu, B. Tang, and B. Zhang, J. Phys. Chem. A **114**, 6188 (2010).
[8] B. Tang and B. Zhang, Chem. Phys. Lett. **412**, 145 (2005).
[9] P. J. Liu, B. F. Tang, and B. Zhang, Chem. Phys. **340**, 141 (2007).
[10] Y. M. Wang, S. Zhang, Z. R. Wei, Q. S. Zheng, and B. Zhang, J. Chem. Phys. **125**, 184307 (2006).
[11] D. N. Zhou, R. Mao, L. M. Zhang, Q. Zhang, and Y. Chen, Chin. J. Chem. Phys. **24**, 647 (2011).
[12] Z. R. Wei, Y. Tang, Q. S. Zheng, and B. Zhang, Opt. Commun. **265**, 532 (2006).
[13] R. Mao, Q. Zhang, J. Z. Zang, C. He, M. Chen, and Y. Chen, J. Chem. Phys. **135**, 244302 (2011).
[14] R. Mao, Q. Zhang, J. Z. Zang, Z. G. Zhang, C. He, C. B. Qin, and Y. Chen, Chin. J. Chem. Phys. **24**, 631 (2011).
[15] A. T. J. B. Eppink and D. H. Parker, Rev. Sci. Instrum. **68**, 3477 (1997).
[16] J. J. Lin, J. Zhou, W. Shiu, and K. Liu, Rev. Sci. Instrum. **74**, 2495 (2003).
[17] D. Townsend, M. P. Minitti, and A. G. Suits, Rev. Sci. Instrum. **74**, 2530 (2003).
[18] J. L. Li, C. M. Zhang, Q. Zhang, Y. Chen, C. S. Huang, and X. M. Yang, J. Chem. Phys. **134**, 114309 (2011).
[19] B. Y. Chang, R. C. Hoetzlein, J. A. Mueller, J. D. Geiser, and P. L. Houston, Rev. Sci. Instrum. **69**, 1665 (1998).
[20] Y. R. Luo, *Comprehensive Handbook of Chemical Bond Energies*, Boca Raton: CRC Press, (2007).
[21] S. Yang and R. Bersohn, J. Chem. Phys. **61**, 4400 (1974).
[22] Y. J. Jee, Y. J. Jung, and K. H. Jung, J. Chem. Phys. **115**, 9739 (2001).
[23] G. E. Busch and K. R. Wilson, J. Chem. Phys. **56**, 3638 (1972).

DOI:10.1063/1674-0068/26/05/493-497